Powder Technology 284 (2015) 571–584

Contents lists available at ScienceDirect

Powder Technology

journal homepage: www.elsevier.com/locate/powtec

Perspectives

Dense granular flow — A collaborative study

P. Mort [a,*], J.N. Michaels [b,c], R.P. Behringer [d], C.S. Campbell [e], L. Kondic [f], M. Kheiripour Langroudi [g], M. Shattuck [h], J. Tang [i], G.I. Tardos [j], C. Wassgren [k]

[a] Procter & Gamble Co., Cincinnati, OH, USA
[b] Department of Chemical Engineering, University of Delaware, Newark, DE, USA
[c] International Fine Particle Research Institute, Wilmington, DE, USA
[d] Department of Physics, Center for Nonlinear and Complex Systems, Duke University, Durham, NC, USA
[e] Aerospace and Mechanical Engineering, University of Southern California, Los Angeles, CA, USA
[f] Department of Mathematical Sciences and Center for Applied Mathematics and Statistics, New Jersey Institute of Technology, Newark, NJ, USA
[g] Merck & Co., Inc., West Point, PA, USA
[h] Benjamin Levich Institute and Department of Physics, The City College of the City University of New York, NY, USA
[i] TGS-Nopec Geophysical Co., Houston, TX, USA
[j] Department of Chemical Engineering, The City College of the City University of New York, NY, USA
[k] School of Mechanical Engineering, Purdue University, West Lafayette, IN, USA

ARTICLE INFO

Article history:
Received 30 September 2014
Received in revised form 27 May 2015
Accepted 1 June 2015
Available online 6 June 2015

Keywords:
Dense granular flow
Granular rheology
Jamming
Hopper
Couette
Collaboration

ABSTRACT

The International Fine Powder Research Institute (IFPRI) has funded an extensive program in dry powder and granular flows, including a focused study on dense flows of interest to a range of industrial handling and process unit operations, especially dense flows at relatively high shear rates. The dense flow program included experimental studies of granular rheology in 3D axial Couette and 2D hopper geometries, wherein the effect of force chains and jamming interactions were investigated as relevant to flow, stress and packing dynamics. The program cumulated in a collaborative study funded by the NSF, wherein a group of academic collaborators was invited to model experimental systems used in IFPRI-sponsored projects. This paper provides a summary of the IFPRI program, details of the collaborative modeling study, and perspective on what is needed to progress the work further.

1. Background

The International Fine Particle Research Institute (IFPRI), a consortium of industrial companies and academics, has supported through pooled industrial funding a rich program of research in particulate flow extending over 35 years (Appendix 1). Over the past decade, much of IFPRI's focus on particulate rheology has been toward understanding and manipulation of flow and stress fields in granular and powder materials across industrially relevant process conditions, i.e., as a function of operating conditions, material properties, and particulate characteristics. In one aspect associated with process throughput of granular solids, there are opportunities in gaining insight into efficiencies associated with fluid-like rheology of granules having a relatively high bulk packing fraction and high shear rate. While there is a good body of engineering and science for very slow, dense-packed flows (friction analogies based on soil mechanics principles), and a good body of work for very rapid, dilute flows (gas-like analogy), there is relatively little work in the intermediate regime.

Classification of dry particulate flow regimes has been done in several ways and is dependent on applications [1–5]. Overall, we can consider a quasi-static regime with friction-like flow behavior, an intermediate (or elastic–inertial) regime having particles with concentrated packing structure and high enough shear rate to incite transient contact networks, and a rapid-kinetic (or inertial–collisional) regime with relatively dilute conditions characterized by binary particle interactions. In the quasi-static regime, stress is independent of the strain rate; in the inertial–collisional regime, the stress scales as the square of the strain rate [6]. In between these two regimes is an intermediate regime where stress is related to the strain rate in the form of a power law [7]. The transition from intermediate to inertial–collisional has been characterized as a dense-inertial regime having clusters of particles whose

* Corresponding author. Tel.: +1 513 377 7910.
E-mail addresses: mort.pr@pg.com (P. Mort), ifpri.vp@verizon.net (J.N. Michaels), bob@phy.duke.edu (R.P. Behringer), campbell@usc.edu (C.S. Campbell), kondic@njit.edu (L. Kondic), mehrdad.kheiripour@merck.com (M. Kheiripour Langroudi), shattuck@ccny.cuny.edu (M. Shattuck), Tyler.Tang@tgs.com (J. Tang), gtardos@ccny.cuny.edu (G.I. Tardos), wassgren@purdue.edu (C. Wassgren).

http://dx.doi.org/10.1016/j.powtec.2015.06.006
0032-5910/

structure has little effect on the stress transmission [8]. The transition from collisional to intermediate flow, i.e., the onset of stress-bearing networks, is very sensitive to packing fraction and boundary conditions.

Particulate flow regimes are of interest over a range of applications:

- Quasi-static flows are applicable to bulk storage and handling. Jenike's analysis [9] predicts the necessary conditions for onset and type of flow pattern in a hopper that may have multiple regimes including entirely static regions, flowing regions, and empty regions.
- At the other extreme, fluidization is heavily dependent on the interaction of particles with a gas flow; rapid flow in risers can be approximated using kinetic theories with fluctuation terms (i.e., granular temperature) and turbulence contributing to the description of bubbling, clustering, and streaming phenomena. While there remains some debate on the measurement and modeling of fluctuations in gas-fluidized systems [10,11], a range of useful modeling methodologies have been developed for well-fluidized systems [12,13]. Additionally, Geldart's empirical classification [14] relating particle size to the density difference between the gas and solid phases remains useful for many fluidized bed applications.
- The focus of the current work is the intermediate regime having relatively dense flows of particles in significant shear flow, typically with transient, multiple contacts, i.e., force chains in an evolving network. Stress fluctuations in dense flows may originate from the transient behavior of stress-bearing networks, i.e., the dynamics of network formation and breakage. In one aspect of this rheology, stress-bearing particle networks and transient jamming may lead to build up of material on boundaries and even clogging of industrial devices. In another aspect, transient networks are crucial to the efficient transmission of stress in a dense granular flow, for example in dense conveying or in a convective flow through a mechanical mixer or reactor. In yet another aspect, fluctuations in structure are critical to particle-scale interactions including micro-mixing and dispersion in dense flows.

In 2006 and 2007, IFPRI commissioned two research projects aimed at dense, intermediate flow: Constitutive Characterization of Dense Flows in the Intermediate Regime (Prof. G. I. Tardos and Dr. M. Kheiripour Langroudi), and Dynamics and Rheology of Cohesive and Deformable Granular Materials (Prof. R. P. Behringer and Dr. Junyao Tang). The Tardos project was engineering-based, suitable for both model and industrial materials, consisting of a full 3D bulk flow device (i.e., an axial Couette-flow) instrumented to measure normal and shear stress components of the bulk flow along with solids packing fraction in the shear gap. The Behringer project used a variety of imaging techniques to investigate the micro-structural aspects of photo-elastic particle flows in 2D hoppers, specifically packing and velocity fluctuations, dynamics of jamming, and probability of clogging. While particle-scale and force-chain physics revealed by the 2D experiments (Behringer) are relevant to the bulk flow and stress fields measured in the 3D axial Couette (Tardos), the physical connection of the two programs was not achieved through experimental collaboration. Modeling efforts were proposed to help bridge this gap.

In 2010, with support of the U.S. National Science Foundation (NSF), the study was expanded to include additional participants with expertise in modeling and simulation. The scope of the NSF grant included support for modeling and a Collaboratory Workshop adjacent to the 2011 IFPRI meeting. The first goal was to see how well the 2D Hopper and axial Couette datasets could be replicated by existing simulation techniques. This effort was to not only assess modeling accuracy, but to see what insights the modeling could give to the experiments. A further goal was to span the two datasets, relating the micro-mechanics elucidated by the 2D study to the bulk-rheology characterization in the 3D Couette experiments. A summary of the Collaboratory, lessons learned about its process, and future recommendations are detailed in Appendix 2.

The Collaboratory includes coordinated work by Profs. L. Kondic and M. Shattuck using discrete element method (DEM) modeling to simulate the 2D hopper experiments and independent work by Profs. C. Campbell and C. Wassgren using DEM to simulate the 3D Couette experiments. Additionally, results of several other collaborations using various continuum approaches to simulate the 3D flows and/or using rheological data obtained in the axial Couette experiment to model other flow geometries are reviewed.

2. Experimental, 2D hopper flow

Two categories of 2D hopper data were included in the Collaboratory. The first category consisted of measurements for: 1) mean time to empty the hopper; 2) mass flow rate; and 3) mean survival time for flow without a jam sufficient to clog the flow. Data in the second category describe the flow locally within the hopper, including: 1) local density, 2) local flow velocity, and 3) local stress.

The 2D hopper developed by Behringer and Tang (Fig. 1) comprises a pair of Plexiglas plates that are spaced slightly more than the thickness of disk-shaped particles. Particles are made from approximately 0.32 cm thick polymer sheet, PSM, manufactured by Vishay Inc. for photo-elastic observations. The diameter of the disks is either 0.770 cm or 0.602 cm, with 62% by number of the sample consisting of the smaller diameter particles. In total, there are approximately 8750 of these disks. The nominal elastic modulus of the particles is 4.8 MPa, nominal solid density is 1.15 g/ml, and the static friction coefficient is ~0.7 to 0.8.

The hopper is formed from pairs of aluminum plates which can be moved laterally so as to change the opening size at the bottom of the hopper. In addition, the hopper opening is closed by a pair of slats that can be pulled open in order to initiate flow. The width of the hopper is 43 cm and the height above and below the opening is approximately 100 cm.

The mass flow rate, Q, and by inference, the time to empty the hopper are related to the Beverloo equation [15], modified for a 2D system.

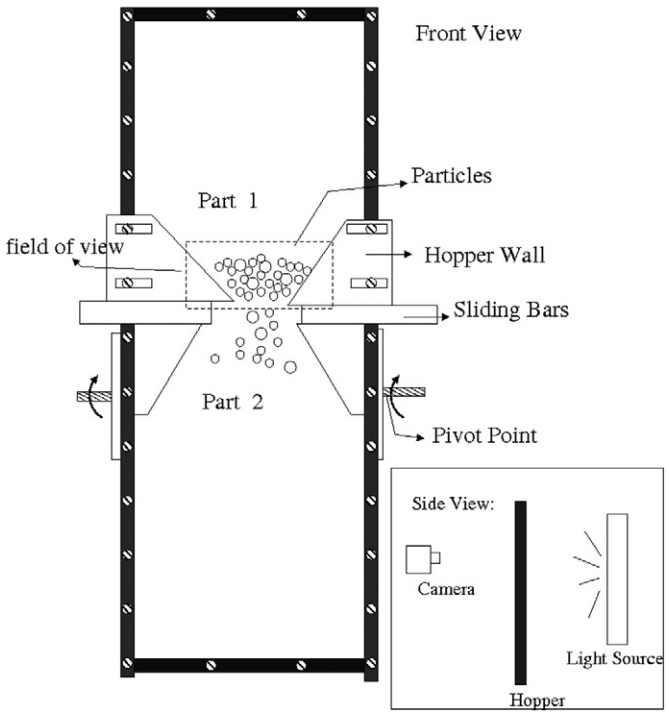

Fig. 1. Schematic of 2D hopper.

This equation has been substantiated by a number of studies in 3D, and it gives the flow rate from a 3D conical hopper of opening of diameter D:

$$Q = C\ \rho_b\ g^{1/2}(D - k\,d_p)^{5/2}. \quad (1)$$

Here, g is the acceleration due to gravity, ρ_b is the bulk density of the material at the hopper exit, and d_p is an effective grain diameter (d_p = 6.7 mm). The parameters C and k are constants that are determined by fitting experimental data for a given material and hopper geometry. The interpretation of the Beverloo equation is fairly simple. During outflow, the mass flux is $J = \rho_b U$, where U is the typical speed of the material at the funnel outlet. In the simplest scenario, one envisions plug-like flow coming out of the funnel. The mass flow is $dM/dt = JA = Q$, where $A \sim D^2$ is the area of the hopper opening. The key piece of insight here concerns U. One imagines that material fluidizes up to a height ~ D in the hopper. Hence, the exit speed corresponds to the free-flight of material that started from rest and fell under gravity by D:

$$U \sim (gD)^{1/2}. \quad (2)$$

However, the process is restricted by drag at the walls, and there is a boundary layer effect which reduces D to an effective value depending on the particle size. Thus, D is replaced by $(D–kd_p)$. In the 2D case with a rectangular orifice, where h is the disk-particle thickness and ν is the packing fraction, the hopper opening varies as the first power of D (D is the exit width; $D \gg h$), and the 2D Beverloo equation becomes:

$$Q = (4/\pi)C\ \nu\ \rho_s\ g^{1/2}h(D-kd_p)^{3/2}. \quad (3)$$

Re-arranging Eq. (3) provides a linear relationship between the mass flow rate, $Q^{(2/3)}$, and the orifice size, D, shown graphically in Fig. 2a. Linear regression of the data according to Eq. (4) provides values of "C" (derived from the regression slope) and "k" (derived from the x-intercept); notice that the x-intercept does not significantly vary with the hopper half angle, α.

$$Q^{2/3}/d_p = \left[(4/\pi)C\ \nu\ \rho_s\ g^{1/2}h\right]^{2/3}(D/d_p - k). \quad (4)$$

The increase in discharge flow rate with decreasing hopper half-angle is consistent with an earlier review of 3D flows in rectangular hoppers where the length of the slot is large compared to the width [16]. In the current work, we observe an empirical relation for mass flow rate as a function of hopper half angle expressed in Eq. (5), where the LHS is an effective discharge coefficient depending on hopper half angle (α) having A and B as fit parameters and C_{90} being the equivalent Beverloo coefficient "C" for a flat-bottom hopper (α = 90°):

$$C_{90} + A\ \cot^B(\alpha) = Q/\left[(4/\pi)\nu\ \rho_s\ g^{1/2}h(D-kd_p)^{3/2}\right]. \quad (5)$$

The discharge data are plotted in Fig. 2b according to Eq. (5) with k = 1.48 and a 2D random close-pack assumption, ν = 0.84. Under these conditions, the best-fit parameters are: C_{90} = 0.587, A = 0.0781, and B = 1.71; note that the value of C_{90} is consistent with 3D Beverloo analyses of free-flowing granules in flat-bottom hoppers.

While the time to empty a hopper containing a given mass is well predicted by the Beverloo equation, it only applies for orifice sizes that are larger than a critical jamming dimension, and on time scales that are long compared to the characteristic time for a grain to fall a characteristic distance, i.e., its own diameter [17]. In general, velocity, packing fraction, stress, and mass flow rate are all locally fluctuating quantities.

Mechanisms of jam formation and relaxation are of interest in granular rheology. The 2D data were collected over a range of dimensionless orifice sizes and hopper angles, tabulating instances of jamming sufficient to arrest flow at the outlet (Fig. 3). Jamming appears to follow an exponential distribution with the mean time to clog (λ) being a strong function of the dimensionless orifice size. The best exponential fit was obtained relative to the square of the dimensionless orifice size [18], further adjusted by the boundary-layer dimension, k = 1.48. Over the range tested, the hopper half-angle appears to have little effect on the clogging interval.

Further 2D experiments determined local velocity and density fields by particle tracking and high-speed video. For local pressure measurements, photo-elasticity measurements were used in which the particles are placed between crossed polarizers. For each high-speed video image, the gradient squared, G2, of the polarized image intensity is calculated; G2 is then related to the local pressure by means of a calibration [19]. In the calibration, we compress a sample of the grains and determine the value of G2 per particle under the same lighting conditions as the hopper flow experiments.

Coarse graining of flow and pressure fields was accomplished by means of a smoothing function (Eq. (6)) such that the coarse grained value of any field, A(r), with particle positions defined according to subscript notation, r_i, was given by Eq. (7) where the summation is taken over all particles (i = 1…N) and the integral is evaluated in two dimensions, hence the dr'^2 notation. Values of w from 1 to 3 mean that the grain diameters gave comparable results.

$$\psi(r-r') = (\pi w)^{-1}\exp\left\{-[(r-r')/w]^{-2}\right\} \quad (6)$$

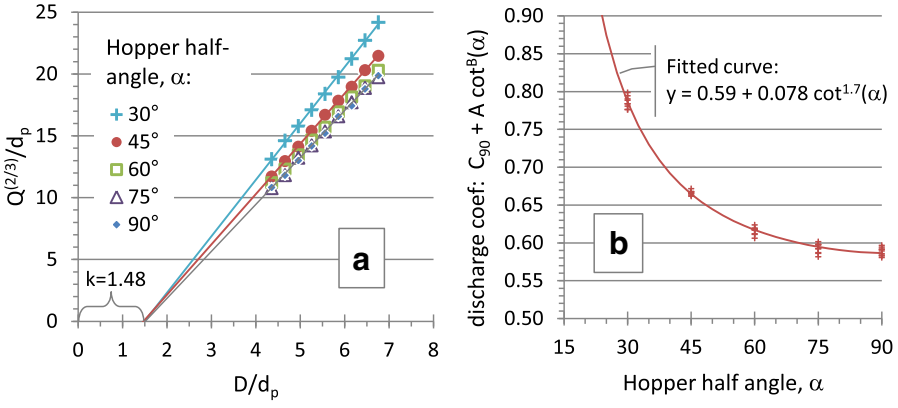

Fig. 2. a) Flow rate data for hopper discharge at different half-angles (from vertical) plotted according to Eq. (4); b) discharge coefficient as a function of hopper half angle plotted according to Eq. (5) with k = 1.48, and assuming random close packing, ν = 0.84.

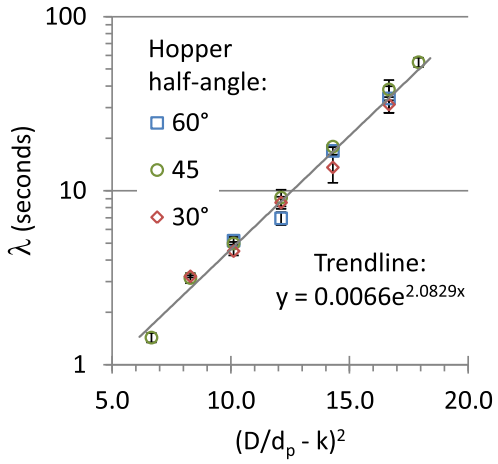

Fig. 3. Jamming data summarized as the mean time interval (λ) between jams sufficient to clog the outlet as a function of dimensionless orifice size reduced by Beverloo "k" coefficient.

$$A(r) = \int \psi\left(r - r'\right) \sum A\left(r' - r_i(t)\right) dr'^2 \tag{7}$$

For instance, in two cases of relevance here, the mass density (Eq. (8)) and momentum density (Eq. (9)) are given at the 'microscopic' or grain scale where m_i and v_i are the mass and velocity of particle i, and the summation is taken over all particles. Here, $\delta(r)$ is the Dirac delta function.

$$\rho(r,t) = \sum m_i \delta(r - r_i) \tag{8}$$

$$p(r,t) = \sum m_i u_i \delta(r - r_i) \tag{9}$$

The coarse grained, hence smoothed, fields are similar to the microscopic fields, except that the delta functions are replaced everywhere, as the result of the convolution, by the smoothing function, $\psi(r - r')$. Note that we have chosen a Gaussian smoothing function, but other choices are possible and give similar results. The local coarse grained velocity, U(r,t) is obtained from the smoothed momentum and density fields (Eq. (10)).

$$U(r,t) = \frac{p(r,t)}{\rho(r,t)} = \frac{\sum m_i u_i \psi(r - r_i)}{\sum m_i \psi(r - r_i)} \tag{10}$$

We used this approach for obtaining a coarse grained velocity because ρ(r,t) and p(r,t) correspond to conserved variables, whereas U(r,t) is a derived variable, which by itself does not satisfy a conservation law. We obtain coarse grained pressure fields in the same general manner as the coarse grained density. Note that the kinetic stress is not included in the experimental data displayed in Fig. 4. The kinetic stress, proportional to ρU^2, is approximately 2 orders of magnitude less than the contact stress distribution throughout most of the hopper.

Fig. 4 shows discharge in a 30° half angle (from vertical) hopper, both in flow and stress fields. While the average velocity (Fig. 4a) is greatest in the region extending through the orifice and extending up into the cone, the velocity fluctuation (Fig. 4b) is highest in an arch pattern just above the outlet, where jamming may have sufficient stability to cause clogging. The minimum in the average stress field (Fig. 4c) approximately coincides with the maximum average velocity. Stress fluctuations (Fig. 4d) are consistent with the average stress field, with magnitude comparable to the mean, i.e., the relative stress fluctuation is quite significant. Fig. 5 shows a similar set of flow and stress fields for a hopper having a 75° half angle. While its flow fields are similar, the particle stresses and their fluctuations are much higher in the shallow-bottom hopper.

3. Experimental, 3D axial Couette flow

The 3D axial Couette cell developed by Tardos and Kheiripour (Fig. 6a) has a vertical shear gap between the rotating and the stationary cylinders. The walls of the Couette are made rough by gluing sand paper on the shearing surfaces as shown in the figure. The roughness of the walls is chosen to match or exceed the coefficient of internal friction of the material thereby trying to assure a non-slip boundary condition. The material above the rotating cylinder (denoted overburden in the figure) is stationary and only provides dead weight to the shearing layer. The Couette can be operated in batch mode (with the valve on the bottom closed) or in continuous mode with an axial flow by removing a small amount of powder (typically ~200 g/min) through the

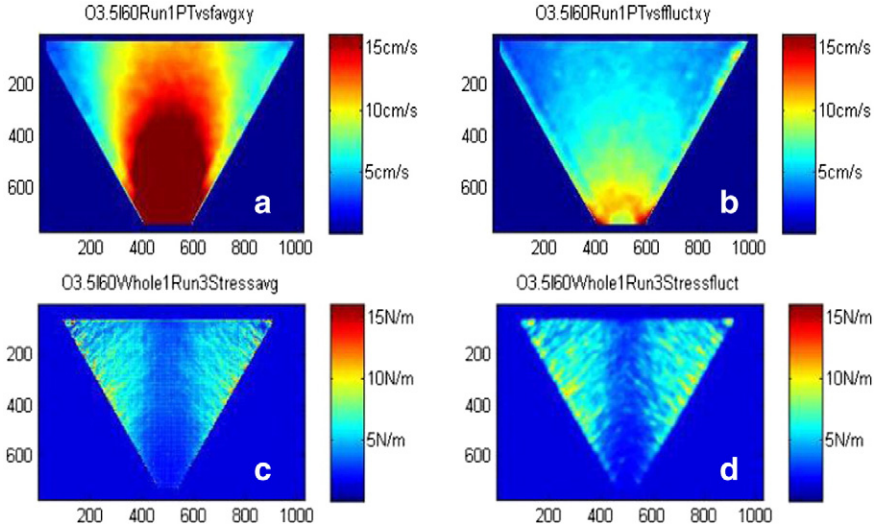

Fig. 4. Experimental velocity and stress fields in 2D hopper with half-angle 30° from vertical, i.e., a "mass flow" condition: a) average velocity; b) velocity fluctuation; c) average stress; d) stress fluctuation.

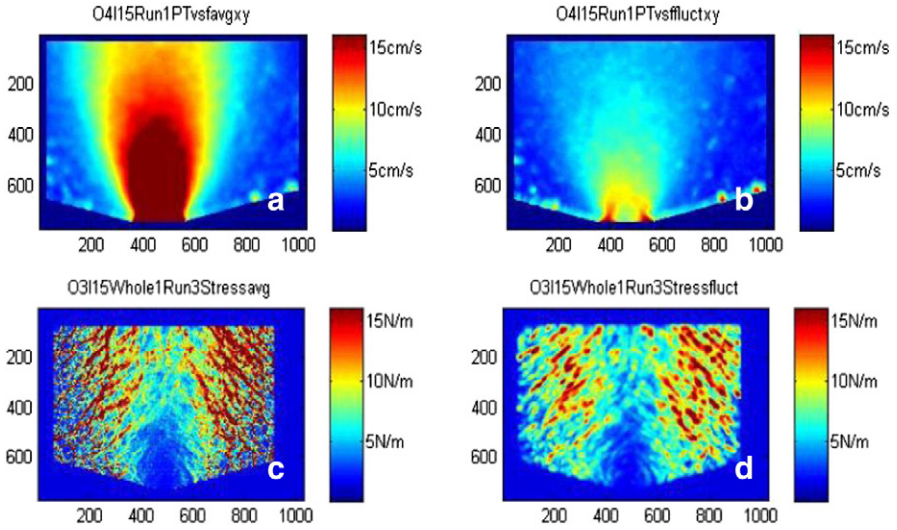

Fig. 5. Experimental velocity and stress fields in 2D hopper with half-angle 75° from vertical, i.e., a "funnel flow" condition: a) average velocity; b) velocity fluctuation; c) average stress; d) stress fluctuation.

bottom and feeding the same amount at the top so as to keep the overburden at a constant level above the rotating cylinder. More detail about the operation of the device is given elsewhere [20].

For each rotational speed, three sets of data were measured: torque, normal stresses with a stress transducer mounted in the middle of the rotating cylinder (sensor diameter 9.53 mm), and solid fraction data using a capacitance probe. Solid fraction data were taken in one of two positions: flush to the outer wall and 6 mm from the rotating wall by inserting the capacitance probe (~1 cm diameter) into the active shearing zone. The capacitance probe detects an approximately hemispherical volume of ~3 mm radius at its end.

Note that torque and normal stress data were collected at different rates according to their individual sensors. These data were reconciled to assure that normal stress data collected at a much higher rate corresponded to torque data taken at slower rate but over the same time period. This methodology allows analysis of stress fluctuations according to the normal stress sensor and convective shear transmission according to the torque data (Fig. 7). Converting the rotation speed (RPM) to shear rate ($\dot{\gamma}$, Eq. (11)) and torque (T) to shear stress (τ, Eq. (12)), a power-law rheology is obtained (Eq. (13), Fig. 8), where φ is the slow-flow (quasi-static) internal friction angle and b and n are shear-rate dependent coefficients.

$$\dot{\gamma} = \frac{2 \times \mathrm{RPM}}{60(D_{out} - D_{in})} \tag{11}$$

$$\tau = \frac{2 \times T}{\pi \cdot D_{in}^{\,2} \cdot L} \tag{12}$$

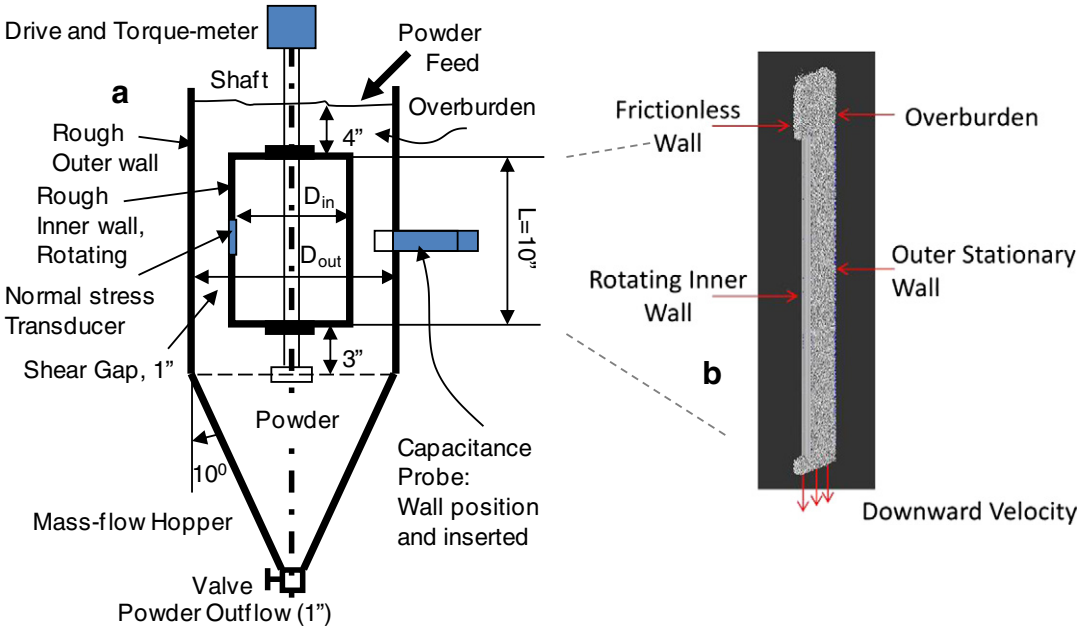

Fig. 6. Schematic of 3D axial Couette: a) continuous experimental set-up with 1″ shear gap, $D_{in} = 4''$, $D_{out} = 6''$; b) simulation slice used by Campbell.

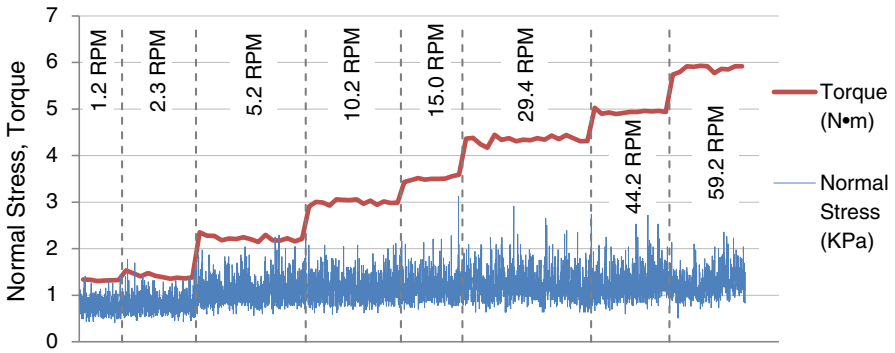

Fig. 7. Normal stress and Torque data for 1 mm glass beads measured over a series of rotational speeds in the axial Couette cell operating in the continuous flow mode. The torque measurement is averaged over the full volume of material in the shear gap. The normal stress sensor is localized, and its acquisition speed is much faster than the torque sensor. The abscissa represents data values collected over time.

$$\tau/\sigma = \tan(\varphi) + b\dot{\gamma}^n \quad (13)$$

In order to obtain solid packing fraction data, the capacitance probe was calibrated at given solid fractions using the particles' dielectric properties. Calibration was done using batch mode (no powder flow vertically through the shear layer), where the packing fraction can be independently calculated based on the fill height and mass of particles added. For model glass bead materials tested in batch mode, the packing fraction increased with time (Fig. 9) until the packing fraction at the outer wall reached a plateau at ~64% with very little fluctuation, indicative of jammed close-packing; note that this packing fraction was independent of rotation speed tested.

In continuous mode, the particle's packing has freedom to dilate with the axial flow, showing fluctuations in packing fraction at both probe positions (Fig. 10). As the rotational shear increases, an apparent gradient develops between the inner and outer walls of the Couette. With increasing shear rate, a close-packed boundary layer appears to form at the stationary outer wall, while the packing near the inner (moving) boundary appears to reduce slightly, but with fluctuations that increase with the shear rate. In the case of the 6 mm gap data, it is speculated that the probe's insertion may affect the flow (i.e., as an intruder), contributing to the measured fluctuations.

While the measured fluctuations in packing fraction (Fig. 10) are much higher than the torque fluctuations (Fig. 7), it must be noted that each sensor's scale of scrutiny is different. The torque measurement integrates the rheology over the sample volume in the gap, extending its full circumference and height, with a volume of over 2 l; in the case of 1 mm glass beads, over 2 million particles are in the gap. In comparison, the capacitance measurement of packing fraction is localized at the tip of the capacitance probe, with a sampling volume of only ~0.06 ml, roughly 60 particles; its scale of scrutiny is more similar to the normal stress sensor that is mounted on the inner wall.

4. Modeling and simulation

Discrete element method (DEM) modeling has been used to simulate granular flow in a variety of applications [21–26]. DEM has the advantage of treating interactions of multiple particles and their boundary conditions. Specifically, DEM has the ability to predict detailed behavior on a meso-scale, including collisions, stress-network statistics, and localized fluctuation in stress and packing. On the other hand, there are practical limits to the size of the system that can be interrogated with DEM, and limits to the breadth of size distributions. For this reason, theoretical work and experimental collaboration with DEM simulators tend to use relatively mono-disperse spherical particles (e.g., glass beads, or similar with reduced stiffness) as model systems. To further simplify modeling, large granular packets have been used to represent clusters of particles [27]. DEM models require detailed information on particle properties and parameters for contact interactions (frictional coefficients, restitution, and stiffness modulus).

Continuum modeling approaches using constitutive relations are useful in extending measurements from one device to the prediction of flow in other geometries. Continuum models require input parameters corresponding to the constitutive models being used. In the current work, the 3D Couette is used to develop intermediate-flow constitutive models based on a power-law rheology for stress as a function of strain rate, i.e., shown by the data in Fig. 8.

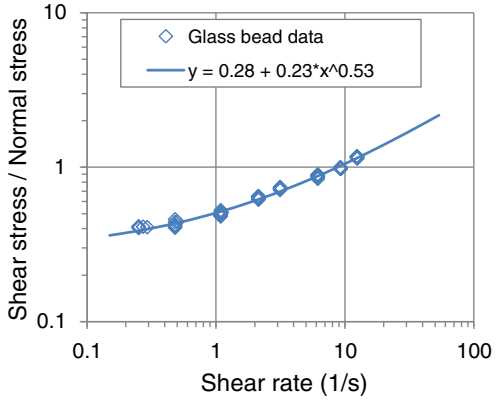

Fig. 8. Rheological power-law fit for average-value glass bead data given in Fig. 7. The power law rheology (Eq. (13)) is fitted using $\tan(\varphi) = 0.28$, $b = 0.23$ and $n = 0.53$.

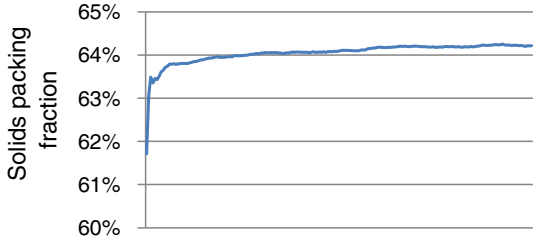

Fig. 9. Solids' packing fraction calibration of capacitance sensor data with 1 mm glass beads, Couette in batch mode operation (no axial flow); abscissa represents time.

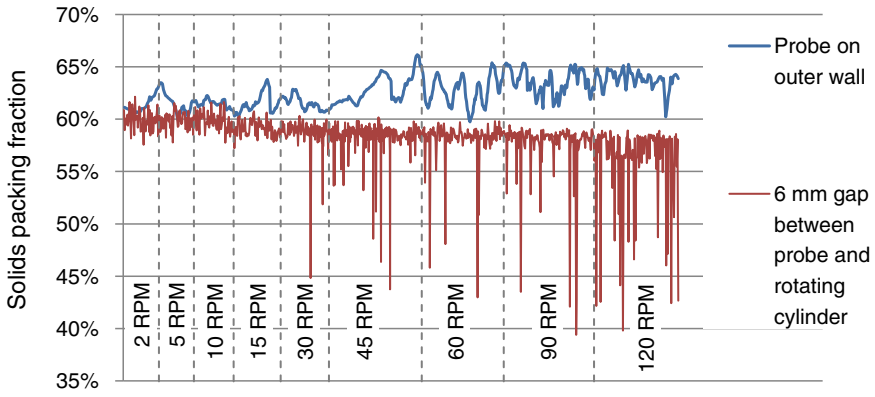

Fig. 10. Dynamic packing fraction of 1 mm glass beads as a function of rotational shear, continuous flow in axial Couette (25.4 mm gap). The graph is an overlay of separate measurements collected over sequential time series at rotational speeds noted.

4.1. 2D hopper discharge and jamming

Kondic and Shattuck ran two types of simulations in comparison to the 2D dataset: 1) volume flux comparisons using a relatively large dimensionless orifice; and 2) clogging probability with relatively small dimensionless orifices. Each simulator used code that replicated the 2D experimental system, implementing equations of motion with force and inertial balances [28]. The Shattuck model used a velocity dependent coefficient of restitution [29].

Volume flux studies considered the time-to-empty the 2D hopper containing a volume of disk particles (same as the experimental system) as a function of the orifice size, made dimensionless by the particle diameter (D/d_p). As a means to calibrate the model's parameters to the experiment, the time to empty the hopper was measured over a range of particle friction and restitution coefficients (Fig. 11). The particles' static friction coefficient had a marginal effect on the emptying time. The particles' restitution coefficient had only weak affects on flux. Comparisons between model and experimental results were done for relatively large orifice sizes ($D/d_p \geq 4.5$), i.e., without clogging. Flux simulations were similar, but marginally faster compared to experimental data (simulated emptying time ranged from 12.2 to 13.4 s; experimental emptying time was 15.87 +/− 0.05 s).

The simulated flow rates followed the 2D Beverloo relationship (Eq. (3)) and were consistent with experiments showing increasing flux with steeper hoppers. However, analysis of the flux in terms of Beverloo parameters showed differences between simulation and experiment. In the simulations, the value of the Beverloo "k" coefficient trended with the hopper half angle (Fig. 12). In contrast, the experimental results showed a constant value of "k" independent of the hopper angle (Fig. 2a).

The study of jamming evaluated the distribution of survival times between jamming events with arrested flow (i.e., clogs) as a function of dimensionless orifice size and hopper half-angle. The survival time (λ) is the time between clogs, where the jams form stable arches at the outlet. In this regime, the material parameters become very important; both energy dissipation (i.e., restitution coefficient must be <1) and a model having static friction were necessary to create jams with stable arches.

The comparative study focused on configurations with relatively small dimensionless orifice sizes where clogging occurs with reasonable frequency; nevertheless, it was necessary to carry out a large number of independent realizations in order to obtain statistically meaningful results. In this aspect, the evaluation of jamming statistics as measured by arrested-flow was tedious; it begs the question of how to better evaluate statistics (experimental and simulation) that are relevant to jamming and other fluctuations in the stress and flow fields.

For relatively small dimensionless orifices ($D/d_p < 4$), the averaged results obtained from these realizations (40 realizations for each case of opening size, D, and half angle, α) showed an exponential trend in the distribution of survival times. When scaled with D and the half-angle dependent "k" values, the survival time realizations for shallow hopper angles ($\alpha \geq 60°$) are remarkably consistent with the exponential trend seen in experiments (Fig. 13). On the other hand, simulations seem to under-predict survival times for steeper hoppers.

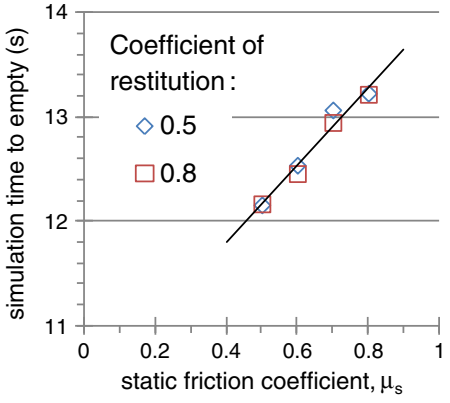

Fig. 11. Calibration of 2D hopper simulations by adjustment of particle friction and restitution parameters. Simulated emptying times are marginally faster compared to experimental results: 15.87 +/− 0.05 s.

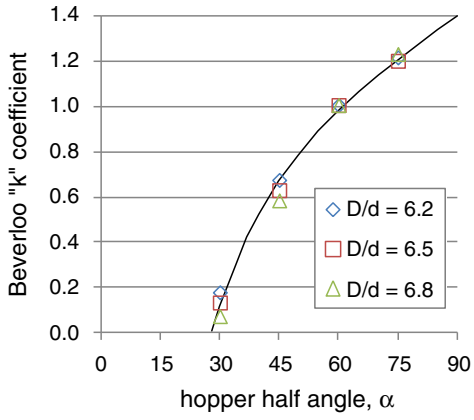

Fig. 12. Dependence on Beverloo "k" coefficient with hopper half angle (from vertical) derived by fitting 2D hopper model data to Eq. (3).

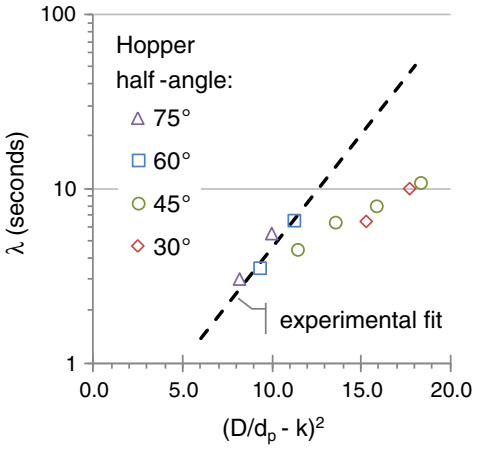

Fig. 13. Comparison of 2D hopper modeling results for the mean time interval (λ) between jams sufficient to clog the outlet as a function of dimensionless orifice size reduced by Beverloo "k" coefficient. The dashed line is the experimental fit obtained in Fig. 3.

Clogging probability itself appears to be independent of the number of particles remaining in the hopper, or at least any variation of this probability is within the statistical variation of the results. When larger openings are considered, such that clogging is possible but not probable, the quality of the exponential fit is rather weak, suggesting that very large numbers of realizations would be needed to either prove or disprove the proposed exponential law. In the case of even larger openings, clogging does not occur, and the outflow of particles is continuous. For the considered bi-disperse distribution of particle sizes, the critical value of the hopper opening, beyond which jamming does not occur, at least for the number or realizations carried out, is found to be between 5 and 6. Both small and large openings lead to the values of the mass flux that are in good agreement with the predictions based on Beverloo's formulation.

Flow and force field realizations were calculated by spatial averaging over cells of size 2×2 (in units of d_p) and time averaging as done in the experimental part of the project. More precisely, the results are first time-averaged over the interval of 1/100 s, and then averaged over the spatial domain of the simulation that is filled with particles. The fluctuation plots show standard deviation of the 1/100 s averages.

Simulations and experiments show good agreement in velocity profiles, both in mean velocity and velocity fluctuation profiles, i.e., comparing Figs. 4 and 14, a & b. We also find a qualitative similarity between stress patterns in experiments (Fig. 4, c & d) and force patterns in simulations (Fig. 14, c & d). However, the simulations predict relatively higher mean force near the wall of the cone and lower force fluctuations, compared to experiments. This result suggests that simulations can provide good agreement with experimentally measured flow dynamics. On the other hand, contact models responsible for stress prediction are in need of enhancement and/or further tuning.

4.2. DEM of 3D axial Couette with periodic volume-limited boundary conditions

Wassgren's group (w/R. Kumar and A. Sarkar) approached the 3D problem as a parametric study using a periodic shear cell with constant volume boundary conditions (i.e., the packing fraction was an input parameter). The periodic shear cell is shown in Fig. 15a. With the goal of matching the experimentally reported shear and normal stress data at 15 RPM ($\dot{\gamma} = 3.14$; $\tau/\sigma \sim 0.70$), they adjusted parameters including elastic modulus (E = 0.1 to 100 MPa), sliding friction coefficient ($\mu_s = 0.01$ to 1), dimensionless rolling friction ($\mu_r/d_p = 0$ to ∞), and packing fraction ($\nu = 0.58, 0.60, 0.62$). While the simulation's periodic boundary conditions accounted for material above and below the cell, the pressure gradient due to gravity was ignored. Static friction was not used in the simulation code. The roughened boundary conditions were modeled by virtually gluing particles to the boundary at various spacing ($s/d_b = 1$ to 2.5).

At higher volume fraction ($\nu > 0.6$) and volume-limited boundary conditions, simulations indicate nearly elastic bulk behavior with normal stress values several orders of magnitude greater than values reported in the experiments. At slightly reduced solid fraction, the simulated normal stresses fall several orders of magnitude, indicating that in the dense regime, stresses are sensitive to even small changes in solid fraction. Similar observations are also reported by Campbell [1], who states that, "… a 2% concentration reduction can be accompanied by nearly three orders of magnitude of stress reduction". Assuming a glass bead modulus of 71 GPa, the scaled value of the normal stress measured experimentally is given by $\sigma_{zz}/E = 1.17$ kPa/71 GPa = 1.65e−8. This is closer to the simulated values obtained for $\nu = 0.58$, suggesting that the solid fraction is smaller in the sheared region.

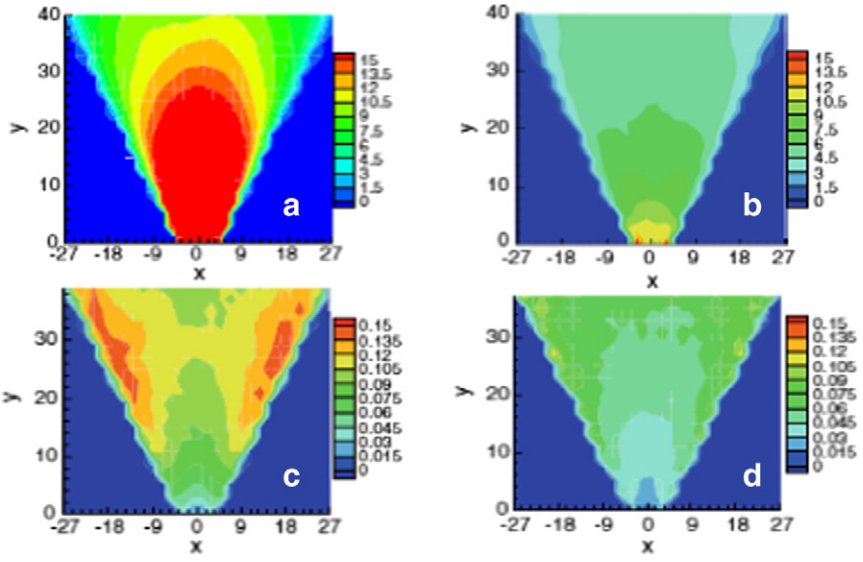

Fig. 14. Simulated velocity and stress fields in 2D hopper with half-angle 30° from vertical: a) average velocity; b) velocity fluctuation; c) average force on a particle; and d) force fluctuation. Velocity data have units of cm/s; force data are in units of particle mass · gravity, where 1 unit = 1.46 mN.

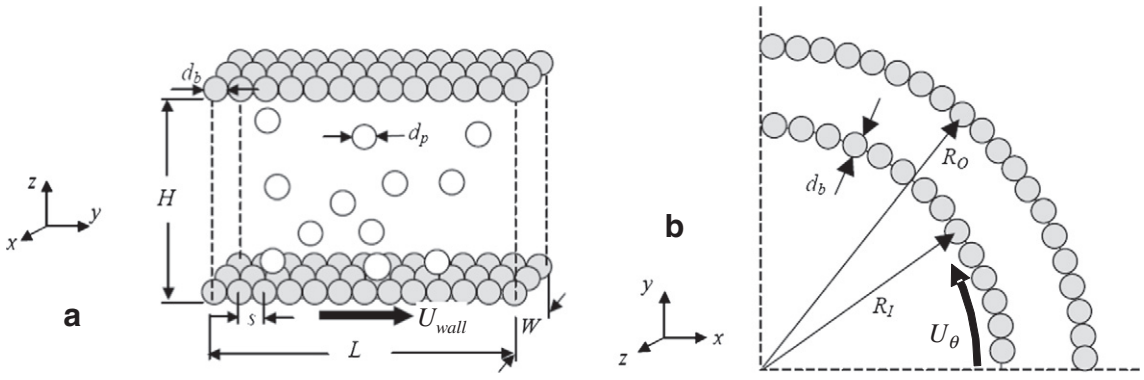

Fig. 15. Schematic of the periodic shear cells used by Wassgren: a) simplified parallel shear cell; b) 90-degree periodic shear cell simulation geometry.

Results for the simulated shear/normal stress ratio (τ_{zy}/σ_{zz} in coordinates of Fig. 15a) trended systematically lower compared to the experimental data (0.73) or fitted rheology model (0.70) in Fig. 8, typically ranging from 0.2 to 0.4 in the parameter studies. A closer match with experiments (Fig. 16) was achieved by eliminating inter-particle rolling, i.e., setting $\mu_r/d_p \to \infty$; in this case, only sliding friction was allowed, $\mu_s = 0.8$. This result suggests the extent to which relatively stiff stress networks can influence transmission of shear stress in the intermediate regime, i.e., the critical characteristic of force chains may be described by the rolling impediment at particle–particle links within a given chain. Alternatively, the tangential force model could have been adjusted to increase its resistance, analogous to the static friction model used in the 2D hopper simulations.

The need to eliminate rolling interactions suggests that there may have been uncontrolled features in the experimental system of 1 mm glass beads. The simulations assumed that the beads were smooth spheres; however, the results suggest that there may have been subtle features such as surface roughness and/or shape eccentricity that impede rolling. To note, other experimental data from the same 3D axial Couette system but with finer glass beads (0.1 mm) show a stress ratio that is closer to Wassgren's simulations with rolling friction, in the range of 0.2 to 0.4 [30].

The effect of the periodic boundary conditions was also tested, comparing simplified parallel shear (Fig. 15a) to a 90° section representing the 3D Couette with axis along z-direction (Fig. 15b). Curved boundary conditions made a statistically significant difference in the simulations, reducing the average shear stress by about 20%.

4.3. DEM of 3D axial Couette with periodic stress-limited boundary conditions

Since the stresses are a product of the overburden and the induced motions in the particle bed, Campbell felt that it was instructive to simulate the entire vertical extent of the experiment, conserving on the number of particles by only simulating a periodic slice as shown in Fig. 6b. The experimental wall boundary conditions using sandpaper with a roughness height roughly equal to the particle diameter was a challenge for simulation because the sandpaper was not well characterized regarding spacing of sand grains, their shape, and their elastic or frictional properties. There was also concern that the backing paper might add compliance to the boundary that could be significant in dense flows of stiff particles (e.g., glass beads). Similar to Wassgren, Campbell chose to simulate the rough boundary using spheres identical in size to the test particles, attached to the wall in a regular hexagonal pattern with a roughness spacing having $s/d_b = 2.0$, allowing test particles to penetrate to the wall between the attached spheres.

Early simulations proved the utility of studying the full system. An examination of the wall stresses showed that the flow was not fully hydrostatic and the Janssen stress on the walls of the Couette was significant; i.e., wall friction supported some of the material overburden. On the other hand, the wall stress continually increases, following an approximately linear trend as the material flows from the top to the bottom of the Couette; it does not approach a constant value as predicted by Janssen theory. Thus, the experiment appears to have a combination of wall friction and hydrostatic effects (Fig. 17).

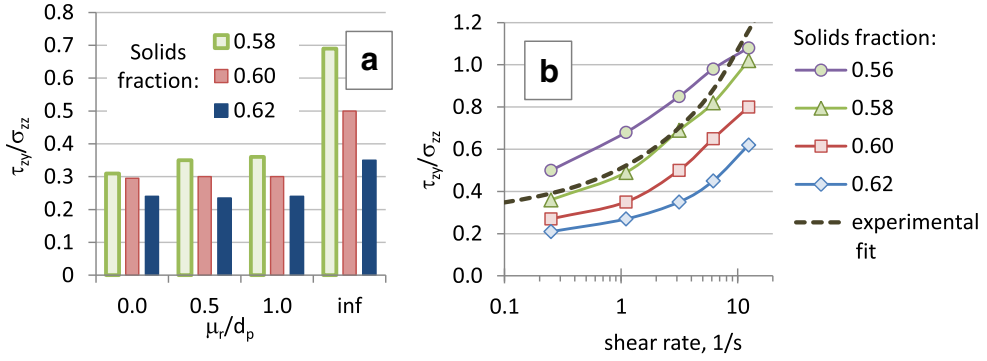

Fig. 16. Convergence of simulations to experimental data: a) best convergence when particles do not roll against each other ($\mu_r/d_p \to \infty$) at 15 RPM; b) predicted shear/normal stress ratio plotted as a function of the shear rate for a range of solid fractions without rolling interactions, i.e., $\mu_r \to \infty$. The dashed line is the experimental fit obtained in Fig. 8.

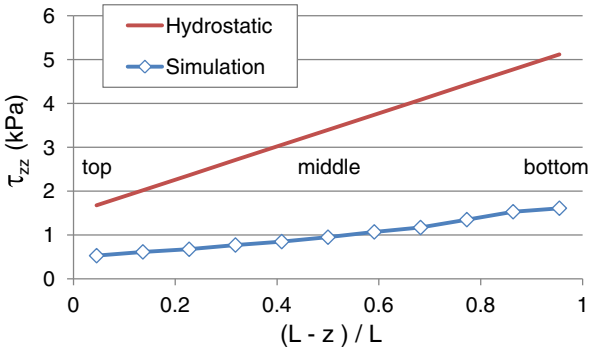

Fig. 17. Illustration of Janssen effect in axial Couette, simulation conditions: 40 RPM, wall roughness spacing $s/d_b = 2.0$.

Initially, Campbell used a novel computational method to simulate the large system (about 160,000 particles in the slice shown in Fig. 6b). Computational load was increased by the small time-step needed to accommodate the stiffness of glass beads (typical E ~ 60 GPa). The initial simulations were run on four 4-core machines, three of which were hyper-threading, allowing 19 simulations to be run simultaneously. To speed up the simulation, a hitherto untried method was used to speed the convergence of the simulation. The first simulations were begun with reduced stiffness (two orders of magnitude smaller than appropriate for glass) and a 10× longer time-step, requiring one tenth of the time to come to convergence. On reaching a converged state, the simulation was restarted and the stiffness slowly ramped up (and the time step ramped down) until reaching a value appropriate for the experimental glass beads. However, even after allowing the simulation to converge for some time, it was found that the average normal stress data were roughly an order of magnitude larger than one would expect from hydrostatic loading. It was surmised that residual stresses were locked into the system and as a result, the convergence is much slower than hoped and much too slow to be completed in the time allowed. The high-stiffness results were discarded and additional simulations were conducted at lower stiffness (E ~ 625 MPa) for inclusion in the Collaboratory.

By simulating the full section of the Couette using particles with reduced particle stiffness, Campbell obtained data relevant to the spatial distribution of shear and stress fields in the 3D device. Representative average velocity and packing fraction data taken from the middle height of the Couette are shown in Fig. 18a. There are several interesting features. Note that there is always velocity slip at the rotating inner cylinder, and much of the material is stagnant with virtually no slip against the outer wall. Perhaps the most noticeable feature in the solid fraction profile is that the solid fraction is reduced where the material is shearing. The radial gradient in solid fraction is also seen experimentally, although not to the same extent: the experimentally-measured shear band was reported to be ~18 particle diameters [31], whereas the simulation results show a much narrower band of about 4–5 particles.

In most cases, the solid fraction is nearly uniform throughout the stagnant region, but interestingly, in profiles near the top of the shear zone, the solid fraction has a maximum just outside the shearing zone (Fig. 18b). While the reason for this is not completely clear, a promising explanation is the generation of a local compression band via centrifugal forces within the shear zone. In a cylindrical system where stress is distributed over a wider area as one moves radially outward, the centrifugal effect would be strongest in the region closer to the inner cylinder. Additionally, note that the solid fraction is reduced next to the outer wall even though the material is stagnant; this is an effect of roughness elements which limit possible packing configurations of particles against the bumpy wall.

In general, increasing the rotation rate of the inner cylinder increases the width of the shearing zone, but only very slightly. The effect is noticeably stronger for boundary conditions with more roughness.

Measured velocities and solid packing fractions are averaged over long periods of time. Over this time averaging, apparently stagnant zones and locally compressed bands may be unsteady, with brief periods of dilation and flow, then resuming a relatively stagnant state, i.e., a quasi-static flow regime having stick-slip behavior.

4.4. Continuum modeling approaches

In addition and in parallel to the work presented in this paper, Tardos and Kheiripour conducted research and collaborations involving continuum modeling of powder flows. During this work, continuum rheological models were derived from data collected using the axial Couette, including packing fraction and normal and shear stresses as a function of shear rate. These models were then implemented in continuum codes to predict flow and stress fields in various geometries including replication of flows in the Couette [20] and predicting stresses and velocity fields in a "spheronizer" geometry [32], i.e., a centripetally-bounded flow with a large free surface and wide shear band.

The motivation for continuum modeling comes from the fact that engineers are quite familiar with concepts of flow of a (Newtonian) fluid including mass and momentum balances and constitutive equations containing material characteristics such as viscosity and density, i.e., the well-known Navier–Stokes equations that are solved to obtain details of the flow field and forces exerted in the flow. Frictional (generally referred as Coulomb) flows of powders are different in that particles

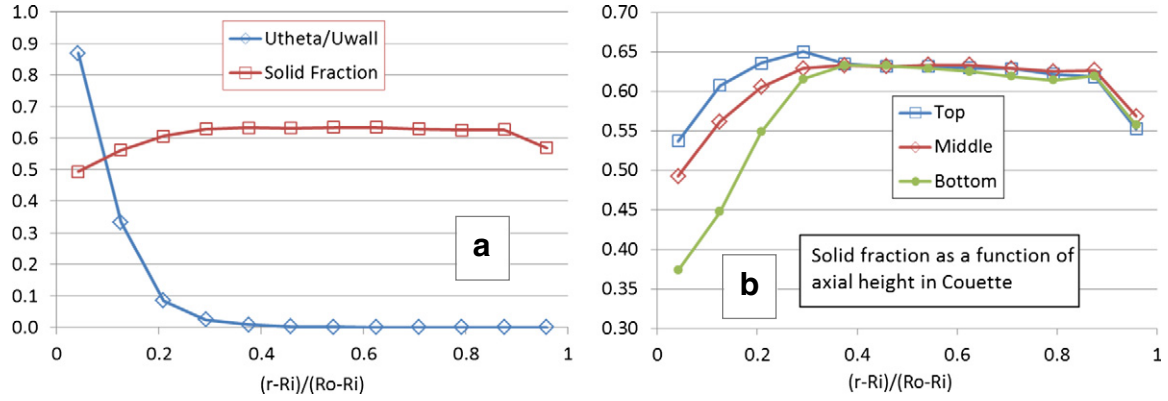

Fig. 18. Results of stress-bounded 3D axial Couette simulations with 1 mm particles (glass beads simulated with reduced stiffness), 40 RPM, wall roughness spacing $s/d_b = 2.0$: a) profile of average tangential velocity (U_θ) relative to the rotating inner wall (U_{wall}) and average solid packing fraction as a function of radial distance in the gap between inner and outer walls measured at middle height position $(L - z) / L = 0.5$; b) solid fraction across the shearing gap, measured at the top, middle and bottom positions of the rotating cylinder.

are in intimate contact and friction is the overwhelming interaction. Thus, while the same mass and momentum balances govern powder and fluid flows, the constitutive equations are different. The goal of the work by Tardos [33–35] and Kheiripour was to develop general equations of motion for bulk powder flows using a fluid mechanics approach [36,37]. Constitutive equations describing the correlation between stress and velocity fields in the axial Couette were employed in the conservation of momentum equation, enabling general equations of bulk rheology that could be applied to other geometries [33]. This approach holds the advantage of being more familiar to a larger segment of the engineering community and especially to students of chemical and mechanical engineering. Further, the format is amenable to stability studies that are essential in obtaining numerical solutions for more complex geometries and, more importantly, amenable to numerical solutions taken from Fluid mechanics.

5. Discussion of flow and stress field correlations

An objective of this study was to relate the micro-mechanics elucidated by the 2D study to the 3D bulk-rheology characterization. A strategy of the Collaboratory was to use modeling as a means to connect scales, from micro-mechanics of particle–particle and particle–boundary interactions, meso-scale interactions of clusters and stress networks, and bulk-scale rheology. An important aspect of dense granular rheology is the fluctuation of stress and flow fields, including their correlation and anti-correlation behavior.

The Collaboratory has 2D data, experimental and simulation, on both micro- and macro-scales. There is reasonably good quantitative agreement between simulations and physical experiments of flux (flow rate) and clogging probability. Additionally, there is good qualitative agreement on velocity spatial distributions and their temporal fluctuations in the 2D hopper. Inferring mechanisms contributing to temporal velocity fluctuations, the data show wave-like patterns in the local packing fraction; dilation waves appears to rise upward in the cone, enabling downward particle acceleration in the wake of the dilation front. This resulting increase in flux is limited at the outlet where transient jams partially interrupt the flow, leading to increased local packing. This observed pattern is somewhat periodic in its dilation/jamming behavior, at least in terms of resultant velocity fluctuations. Speculatively, the cyclical nature of dilation and jamming may be related to the observed clogging probability functionality. Development of statistical tools for comparison of experimental and virtual ensembles, both spatial and temporal, could improve the quantitative basis for model validation and provide a more robust foundation for mechanistic understanding.

There is less consistency regarding prediction of stress fields in 2D flows; compared to experiments, simulations predict lower relative stress fluctuation. In this aspect, additional causal effects of stress networks on rheology (i.e., the extent to which stress networks affect dynamics of local packing and particle velocity) remain uncertain.

The 3D experimental datasets have information on shear stress, normal stress, and packing fraction; however, the data do not directly correlate with regard to the micro or meso-scale aspects of the flow. The shear stress is derived from the measured torque on the bulk flow, evaluated over the full sample volume, while normal stress and packing fraction measurements reflect much smaller sampling volumes at different locations in the axial Couette device. The 3D simulation data show qualitative agreement in flow field behavior, and could be manipulated (i.e., by adjusting friction) to achieve similarity in stress; however, the quantitative details of local packing gradients in the shear gap and fluctuation thereof remain uncertain.

Ideally, one would like to link the micro- and meso-scale information from simulations to the bulk-scale rheology; however, the current experimental work does not allow for direct validation of micro-scale phenomena in the 3D Couette, only by inference to the bulk-scale measurements that are made in separate spatial and temporal reference frames. Direct validation remains a challenge going forward for experimentalists; and better inferential tools could be useful in a modeling context.

From the bulk rheology data, one can infer force chains spanning the shear gap in the 3D axial Couette flow; the force chains resist flow in proportion to a power-law shear rate rheology. While one must be cautious extending 2D hopper observations to the 3D Couette flow, one can infer packing and velocity fluctuations in the downward axial direction of the 3D Couette under continuous flow operation may be analogous to the wave-like patterns observed in the 2D hopper flows. Combining these effects suggests interaction between axial packing fluctuations with the radial and tangential components of force chains; as the shear rate increases, the dynamics of stress network breakage may lag the axial flow, resulting in greater packing fluctuations in the shear gap.

6. Conclusion

The IFPRI program in rheology of dense particulate flows brought focus to intermediate regime flows, having dense packing and flow rates of relevance to many industrial unit operations. Understanding how to control and manipulate dense flows and their associated stress fields can have a positive impact on productivity and quality of systems comprising such operations. From an industrial perspective, exploring a wider range of modeling techniques to describe critical features of flows and boundary-conditions could be helpful, for example, regime mapping and development of scaling rules based on the emerging physics of intermediate flows.

Toward the goal of linking the physics of intermediate flows across the 2D and 3D datasets, this collaborative study showed the need to model transitions between static and dynamic particle interactions. This finding is a common result of both 2D and 3D simulation results. In the case of 2D Hopper flow, including static friction was essential to matching the experimental emptying times over the range of hopper angles tested. In the case of 3D axial Couette flow, the parametric study clearly identified the importance of impeding rolling friction as a means to transmit stress through the granular medium. These findings support the concept of inter-particle contact networks (i.e., force chains) having static-like behavior capable of localized jamming and transmission of stress over finite temporal intervals, where the ability of the system to dynamically form and break such networks on a scale that is comparable to the shear rate is a characteristic of the intermediate regime. Fluctuating stress fields in dense flows remain a challenge for both modeling and experimental measurement. Related studies using continuum rheology, although semi-empirical, suggest that a combination of discrete element and continuum mechanics may be complementary in future collaborations.

Challenges inherent to the study of dense granular rheology persist in bridging micro-, meso- and bulk-scales, along with the comparison of systems based on their ensemble statistics: both flow and stress fields. There is clear value in having a simplified system (i.e. 2D hopper) allowing direct measurement of both local and bulk rheology; development of improved statistical tools for comparison of such experimental and virtual ensembles can improve the quantitative basis for model validation and provide a more robust foundation for mechanistic understanding. Direct validation of local rheology in realistic 3D systems remains a challenge going forward for experimentalists. While one must exercise caution in linking simple and complex systems, multi-scale observations from simplified systems may be useful toward improved mechanistic understanding of granular rheology in realistic systems with more complex materials.

7. Dedication

This paper is dedicated to the memory of Dr. Roger Place. A graduate of Imperial College (Chemical Engineering and Technology, 1961, PhD 1964), Roger's affiliation with the International Fine Particle Research

Institute began as an industrial representative of Tioxide in 1989, and then continuing as IFPRI Vice President and Academic Liaison from 1996 until his passing in 2013. Roger was the principal organizer of the IFPRI-sponsored Powder Flow Workshop (Bremen, Germany, 2003), extending through the Powder Flow Working Group (Appendix 1) and the Collaboratory work presented here. Roger was an active and enthusiastic member of the broader particle technology community, including the AIChE Particle Technology Forum and IChemE Particle Technology Special Interest Group. We will miss Roger's passion and perception, always provoking alternative views and challenging conventional assumptions.

List of symbols used

A, B	Parameters in half-angle dependent hopper discharge coefficient
A(r)	field value, coarse graining
b	pre-exponential factor in power-law rheology
C	Beverloo discharge coefficient
C_{90}	Beverloo coefficient for flat-bottom hopper ($\alpha = 90°$)
D	orifice size
d_b	bead size used to create surface roughness in 3D Couette models
d_p	particle diameter
E	modulus of elasticity
g	gravitational acceleration
h	thickness of disk particles in 2D hopper experiments
i	particle index, coarse graining calculations
k	Beverloo coefficient for boundary layer thickness
L	height of rotating cylinder in 3D axial Couette experiments
n	exponent in power-law rheology
p()	momentum field, coarse graining
Q	mass flow rate
R, r	radial coordinates
s	spacing of beads used to create surface roughness in 3D Couette models
U	velocity
x, y, z	spatial coordinates
α	hopper half-angle, from vertical
$\dot{\gamma}$	shear rate
φ	internal friction angle
λ	time interval between jamming events in 2D hopper experiments
μ_s, μ_r	friction coefficients: static, rolling
ν	solids packing fraction
θ	tangential coordinate
ρ_b, ρ_s	density: bulk, solid
$\rho()$	density field, coarse graining
σ	normal stress
τ	shear stress
$\psi()$	smoothing function, coarse graining

Acknowledgments

This work was funded by the International Fine Particle Research Institute, grant awards FRR0812 and FRR5606, and the US National Science Foundation, grant award NSF1010008.

Appendix 1. IFPRI's support of powder flow research since 1985

Since its inception in 1979, IFPRI has sponsored projects in dry powder flow including fine-powder handling, aerated powder flow, various aspects of fluidization and fluidized-bed reactors, inter-particle forces in dry particle flows, rheological methods applicable to a range of dry flow regimes, pneumatic conveying, mixing, and segregation. In 2004, IFPRI sponsored a Powder Flow Working Group, including both academic and industrial representatives. The Working Group members wrote a series of short articles collected in a review [38] outlining research directions for consideration in advancing fundamental knowledge on powder flow of relevance to chemical, pharmaceutical, civil and mining industries, geophysical sciences, and fundamental research on granular and granular-fluid flows. This review was foundational in the definition of the experimental projects presented in this paper (Tardos, Behringer) and the NSF collaboration with the modeling community.

A list of the IFPRI-sponsored projects in particulate flow is as follows:

- Aerated powder flow; Nedderman, Rathbone (Cambridge) 1985.
- Estimation of powder yield locus & its application to design; Makino (Akita) 1985.
- Method of characterizing the flow of aerated powders; Lloyd, Webb, (Loughborough), 1986.
- Unification of wet, intermediate and dry granular flow — a theoretical approach; Buggisch (Karlsruhe), 1988.
- Characterization and prediction of powder flow; Geldart, Woodcock (Bradford), 1989.
- Granular shear flows: fluid/solid solid interfaces, impact strengths and self-diffusion; Campbell, Zhang (USC), 1992
- Rapid Shear of fine powders; Jackson (Princeton) 1992.
- The discharge of fine powders from Conical hoppers; Nedderman (Cambridge) 1993.
- Turbulent gas–particle flow in vertical risers; Jackson, Sundaresan, Dasgupta (Princeton) 1995.
- Bubble and elutriation control in fluidized beds with electric fields; Colver et al. (Iowa) 1997.
- A review of instrumentation for dense gas–solid flows; Louge (Cornell) 1997.
- Mixing and segregation in industrial processes; de Sliva (Telemark) 1997.
- Measurement of fluidization dynamics in a fluidized bed using capacitance tomography; Beck, Dyakowski, Wang (UMIST) 1998
- Discrete particle simulation of gas–solid flow — effect of inter-particle collision; Tsuji, Tanaka et al. (Osaka) 1998.
- Experimental rapid shear flow; Louge (Cornell) 1998.
- Rapid shear flow of granular materials; Sundaresan (Princeton) 1998.
- Test methods for measuring flow properties of bulk solids, Schwedes (Braunschweig) 1999.
- Suspension paste and powder flow — prospects of a unified approach; Melrose (Cambridge) 1999.
- Characterization of the rheo-mechanical properties of wet-mass powders; Tomas (Magdeburg) 2001.
- Biaxial shear cell; Scarlett, Janssen (Delft) 2000.
- Powder mixing and segregation; Muzzio et al (Rutgers) 2001.
- Study on fundamentals of mixing of powders with emphasis on cohesive systems; Sommer (Munich) 2002.
- Inter-particle forces in powder flow; Pollock & Jones (Lancaster) and Geldart & Verlinden (Bradford) 2002.
- Granular flows in the intermediate regime; Tardos (CUNY) 2002.
- Studies of the fundamental interactions between a gas and agitated particles; Louge et al (Cornell) 2002.
- From wet to dry; Brady (Caltech) 2003.
- Workshop — powder flow in the intermediate regime; Place et al (Bremen) 2003.
- IFPRI Powder Flow Working Group. Academic: Behringer (Duke), Louge (Cornell), McElwaine (Cambridge), Pfeffer (NJIT), Sundaresan (Princeton), Schwedes (TU Braunschweig); Industrial: Jacob (Dow), Halsey (Exxon), Michaels (Merck), Mort (P&G); IFPRI: de Jaeger, Place; NSF: Mountziaris. 2005.
- Mixing of powders and granular materials by mechanical means; Bridgwater (Cambridge) 2008.
- Constitutive characterization of dense flows in the intermediate regime; Tardos (CUNY), 2010.
- Dynamics and rheology of cohesive and deformable granular materials; Behringer (Duke), 2013.

- Effect of tribocharging on powder packing; Castellanos (Sevilla), current.

Appendix 2. Summary and lessons from the Collaboratory

The IFPRI-NSF Collaboratory in Dense Particulate Flow launched in August 2010. A workshop was held adjacent to the IFPRI Annual Meeting in June 2011 (Chapel Hill, NC); attendees included experimental and modeling participants of the Collaboratory along with IFPRI members. The final report for the grant (NSF1010008) was completed in April 2012.

The overarching objective of the Collaboratory was to engage a broader community of industrial and academic researchers, modelers and engineers in defining relevant regimes of dense particulate flow, the underlying physics therein, and the effect of boundary conditions, material properties and particle characteristics on dense granular rheology.

Each of the modeling participants was invited to simulate either the 2D hopper or 3D axial Couette experiments, as described in this paper. Key features of the 2D challenge included prediction of local density, velocity, and pressure fields in the hopper, along with jamming and clogging probability as related to force chains and arch formation. The 3D challenge included prediction of solids fraction, velocity field, normal and shear stress fields, and constitutive relationships between flow and stress fields.

A first goal was to validate and calibrate models against a chosen experimental dataset. Given the 2D hopper with disk particles was a model system, its challenge was to achieve reasonable predictions without parameter adjustment. Recognizing the higher complexity of 3D axial Couette system designed as a rheometer for natural and/or industrial materials, it was anticipated that its models would need tuning using adjustable parameters, for example, describing material properties in the system, i.e., particles and/or boundaries. A second stated goal was to apply the calibrated model to a second system, anticipating that this would seed the overarching objective of the work.

The 2011 Workshop brought participants together face-to-face to discuss experiments, modeling approaches and results. It quickly became apparent that the challenge of addressing the first goal exceeded the Collaboratory's resources. Workshop interactions were very concentrated and set the seed for individual authors on this paper to contribute additional modeling work up to the submission of the final NSF report in 2012; however, it did not allow for productive interaction of the 2D and 3D models. This paper provides closure on the Collaboratory, and documents lessons learned along the way.

Overall, simulations were successful in providing qualitative insight into the internal workings of the experiments. Regarding flow fields, relatively good quantitative agreement was achieved in both 2D and 3D cases. For jamming and arching in 2D, reasonable agreement was achieved with parameter adjustment. Quantitative stress field predictions proved more difficult in both 2D and 3D cases. While the prognosis regarding quantitative prediction of dense granular rheology based on DEM models remains a challenge, the quality of the insight obtained through this study is enough to merit further work

Given that natural and industrially relevant materials comprise an even more challenging range of properties (complex modulus, deformation, cohesion, etc.) and characteristics (shape and size distributions) compared to model materials typically used by academics, it is anticipated that a comprehensive treatment of intermediate regime flows will require substantially greater funding and broader collaborative effort. In the meantime, a wider range of modeling techniques including regime mapping and quasi-continuum modeling could help. In spite of the difficulties in DEM modeling of flows within the 3D axial Couette, its usefulness as an experimental probe of dense-phase rheology makes it relevant for future modeling work.

Of equal importance, much was learned about how to run a collaborative study in the future. Perhaps the most important lesson is that the modelers should have been involved in planning the experiments from the beginning. In a challenge of this scope, critical aspects needing coordination between experimentalists and modelers include the practical implications of selected material properties, particle characteristics, and boundary conditions. The fundamental question of how to approach packing fraction, as a controlled parameter or measured output, is critical in linking experiments and models. Further coordination is advised regarding instrumentation, i.e., the extent that packing, stress, and flow measurements can be correlated, spatially and temporally. Additionally, a multi-scale challenge (e.g., from particle contacts, to force chain and packing fluctuations, to bulk rheology) benefits from coordination of experiments, models, and theoretical hypotheses.

Furthermore, it might help if the modelers were involved in the conceptual design of the experimental program as simplified experiments can elucidate important modeling parameters including contact mechanics in dense flows (normal and tangential), transition between static and kinetic friction, and the effect of particle shape, especially in relation to contact mechanics. Finally, open communication is important; having a series of workshops and/or learning events is useful in bringing participants together, involving modelers earlier in the experimental program, and promoting iterative cross-fertilization of hypotheses, approaches and results.

References

[1] C. Campbell, Granular shear flows at the elastic limit, J. Fluid Mech. 465 (2002) 261–291.
[2] G.D.R. MiDi, On dense granular flows, Eur. Phys. J. E 14 (2004) 341–365.
[3] C. Campbell, Granular material flows — an overview, Powder Technol. 162 (2006) 208–229.
[4] S. Chialvo, J. Sun, S. Sundaresan, Bridging the rheology of granular flows in three regimes, Phys. Rev. E 85 (2012) 021305.
[5] V. Vidyapati, S. Subramaniam, Granular rheology and phase transition: DEM simulations and order-parameter based constitutive model, Chem. Eng. Sci. 72 (2012) 20–34.
[6] R.A. Bagnold, Experiments on a gravity-free dispersion of large solid particles in a Newtonian fluid under shear, Proc. R. Soc. Lond. A 225 (1954) 49–63.
[7] I. Talu, S. McNamara, G.I. Tardos, Slow and intermediate flow of a frictional bulk powder in the Couette geometry, Powder Technol. 131 (2003) 23–39.
[8] C. Campbell, Clusters in dense inertial granular flows, J. Fluid Mech. 687 (2011) 341–359.
[9] A.W. Jenike, Storage and Flow of Solids, Bull. 123, Engineering Experiment Station, University of Utah, 1964.
[10] G. Cody, J. Johri, D. Goldfarb, Dependence of particle fluctuation velocity on gas flow, and particle diameter in gas fluidized beds for monodispersed spheres in the Geldart B and A fluidization regimes, Powder Technol. 182 (2008) 146–170.
[11] J. Wang, M.A. van der Hoef, J.A.M. Kuipers, Particle granular temperature of Geldart A, A/B and B particles in dense gas-fluidized beds, Chem. Eng. Sci. 97 (2013) 264–271.
[12] D. Gidaspow, J. Jung, R. Singh, Hydrodynamics of fluidization using kinetic theory: an emerging paradigm; 2002 Flour–Daniel lecture, Powder Technol. 148 (2004) 123–141.
[13] N.G. Deen, M. Van Sint Annaland, M.A. van der Hoef, J.A.M. Kuipers, Review of discrete particle modeling of fluidized beds, Chem. Eng. Sci. 62 (2007) 28–44.
[14] D. Geldart, Types of gas fluidization, Powder Technol. 7 (1973) 285–292.
[15] W.A. Beverloo, H.A. Leniger, J. Van de Velde, The flow of granular solids through orifices, Chem. Eng. Sci. 15 (1961).
[16] R.M. Nedderman, U. Tuzun, S.B. Savage, G.T. Houlsby, The flow of granular materials — 1, discharge rates from hoppers, Chem. Eng. Sci. 37 (1982) 1597–1609.
[17] A. Janda, R. Harich, I. Zuriguel, D. Maza, P. Cixous, A. Garcimartin, Flow-rate fluctuations in the outpouring of grains from a two-dimensional silo, Phys. Rev. E 79 (2009) 031302.
[18] A. Janda, I. Zuriguel, A. Garcimartin, L.A. Pugnaloni, D. Maza, Jamming and critical outlet size in the discharge of a two-dimensional silo, EPL 84 (2008) 44002.
[19] D. Howell, R.P. Behringer, C. Veje, Stress fluctuations in a 2D granular Couette experiment: a continuous transition, Phys. Rev. Lett. 82 (1999) 5241–5244.
[20] M. Kheiripour Langroudi, S. Turek, A. Ouazzi, G.I. Tardos, An investigation of frictional and collisional powder flows using a unified constitutive equation, Powder Technol. 197 (2010) 91–101.
[21] Y. Muguruma, T. Tanaka, Y. Tsuji, Numerical simulation of particulate flow with liquid bridge between particles (simulation of centrifugal tumbling granulator), Powder Technol. 109 (2000) 49–57.
[22] H. Kuo, P. Knight, D. Parker, M. Adams, J. Seville, Discrete element simulations of a high-shear mixer, Adv. Powder Technol. 15 (2004) 297–309.

[23] R.L. Stewart, J. Bridgwater, Y. Zhou, A.B. Yu, Simulated and measured flow of granules in a bladed mixer — a detailed comparison, Chem. Eng. Sci. 56 (2001) 5457–5471.
[24] B. Remy, T. Canty, J. Khinast, B. Glasser, Experiments and simulations of cohesionless particles with varying roughness in a bladed mixer, Chem. Eng. Sci. 65 (2010) 4557–4571.
[25] J. Li, C. Wassgren, J. Litster, Multi-scale modeling of a spray coating process in a paddle mixer/coater: the effect of particle size distribution on particle segregation and coating uniformity, Chem. Eng. Sci. 95 (2013) 203–210.
[26] H. Nakamura, H. Fujii, S. Watano, Scale-up of high shear mixer-granulator based on discrete element analysis, Powder Technol. 236 (2013) 149–156.
[27] A. Hassanpour, H. Tan, A. Bayly, P. Gopalkrishnan, B. Ng, M. Ghadiri, Analysis of particle motion in a paddle mixer using discrete element method (DEM), Powder Technol. 206 (2011) 189–194.
[28] L. Kondic, Simulations of two dimensional hopper flow, Granul. Matter 16 (2014) 235–242.
[29] J. Schafer, S. Dippel, D.E. Wolf, Force schemes in simulations of granular material, J. Phys. I France 6 (1996) 5–20.
[30] V. Vidyapati, M. Kheiripour Langroudi, J. Sun, S. Sundaresan, G.I. Tardos, S. Subramaniam, Experimental and computational studies of dense granular flow: transition from quasi-static to intermediate regime in a Couette shear device, Powder Technol. 220 (2012) 7–14.
[31] M. Kheiripour Langroudi, P. Mort, G.I. Tardos, Study of powder flow patterns in a Couette cell with axial flow using tracers and solid fraction measurements, Granul. Matter 13 (2011) 541–552.
[32] M. Kheiripour Langroudi, M. Shahnam, J. Michaels, P. Mort, G.I. Tardos, Use of a Couette shearing cell as a powder rheometer to predict stress and flow fields of dense granular matter, AIChE Proceedings 2011, p. 55e.
[33] G.I. Tardos, A fluid mechanics approach to slow, frictional powder flows, Powder Technol. 92 (1997) 61–74.
[34] G.I. Tardos, M.I. Khan, D.J. Schaeffer, Forces on a slowly rotating, rough cylinder in a Couette device containing a dry, frictional powder, Phys. Fluids 10 (2) (1998) 335–341.
[35] G.I. Tardos, S. McNamara, I. Talu, Slow and intermediate flow of a frictional bulk powder in the Couette geometry, Powder Technol. 131 (2003) 23–39.
[36] M. Kheiripour Langroudi, G.I. Tardos, J.N. Michaels, P. Mort, Effect of material properties boundary conditions and flow fields on the rheology of dense granular matter, Powders & Grains, July 2009.
[37] M. Kheripour Langroudi, J. Sun, S. Sundaresan, G.I. Tardos, Transmission of stresses in static and sheared granular beds: the influence of particle size, shearing rate, layer thickness and sensor size, Powder Technol. 203 (2010) 23–32.
[38] R. Behringer, M. Louge, J. McElwaine, P. Mort, R. Pfeffer, S. Sundaresan, Report of the IFPRI Powder Flow Working Group, IFPRI SAR 30-08, 2005 http://www.nsf.gov/eng/cbet/activities/IFPRI-powderflow-SAR30-08.pdf.